Chemical Science

EDGE ARTICLE

View Article Online
View Journal | View Issue

Cite this: *Chem. Sci.*, 2015, **6**, 3797

Highly efficient near ultraviolet organic light-emitting diode based on a *meta*-linked donor–acceptor molecule†

Haichao Liu,[ab] Qing Bai,[ab] Liang Yao,[ab] Haiyan Zhang,[b] Hai Xu,[b] Shitong Zhang,[ab] Weijun Li,[a] Yu Gao,[ab] Jinyu Li,[ab] Ping Lu,[ab] Hongyan Wang,[b] Bing Yang*[ab] and Yuguang Ma[c]

Received 29th March 2015
Accepted 15th May 2015

DOI: 10.1039/c5sc01131k

www.rsc.org/chemicalscience

A novel near ultraviolet (NUV) emitter with a *meta*-linked donor–acceptor (D–A) structure between triphenylamine (TPA) and phenanthroimidazole (PPI), mTPA–PPI, was designed and synthesized. This molecular design is expected to resolve the conflict between the non-red-shifted emission and the introduction of a charge-transfer (CT) state in the D–A system, aiming at NUV organic light-emitting diodes (OLEDs) with high-efficiency and colour-purity. Theoretical calculations and photophysical experiments were implemented to verify the unique excited state properties of mTPA–PPI. The mTPA–PPI device exhibited excellent NUV electroluminescence (EL) performance with an emission peak at 404 nm, a full width at half maximum (FWHM) of only 47 nm corresponding to a CIE coordinate of (0.161, 0.049), and a maximum external quantum efficiency (EQE) of 3.33%, which is among the best results for NUV OLEDs. This work not only demonstrates the promising potential of mTPA–PPI in NUV OLEDs, but also provides a valuable strategy for the rational design of NUV materials by using the *meta*-linked D–A architecture.

Introduction

Near ultraviolet (NUV) emitting materials have attracted considerable attention because of their wide applications in the fields of chemical and biological sensors,[1] high-density information storage,[2] and lighting sources.[3] Furthermore, NUV emitting materials can also be utilized as host materials in doped organic light-emitting diodes (OLEDs), aiming at suppressing the aggregation- or concentration-caused luminescence quenching of fluorescent and phosphorescent emitters.[4] Nevertheless, it is a great challenge to achieve high-performance OLEDs based on NUV emitters, and the external quantum efficiency (EQE) of NUV OLEDs is usually less than 2%, which is mainly ascribed to the intrinsic wide band-gap of NUV emitters that causes unbalanced charge injection and charge transport in OLEDs.[3d,5,6]

Constructing donor–acceptor (D–A) molecules is one of the most commonly used methods to improve the charge injection and carrier transportation of organic semiconductor materials.[7] Especially, in some fluorescent D–A material-based OLEDs, triplet excitons have been demonstrated to be almost fully employed, and even more excellent performances were obtained in such OLEDs.[8,9] D–A compounds usually possess weakly bound charge-transfer (CT) excitons which facilitate a reverse intersystem crossing (RISC) process in the OLEDs. However, it is rather rarely reported that NUV OLEDs based on D–A molecular architecture exhibit high efficiency and favourable colour-purity. Firstly, in principle, D–A molecules are more suited to designing narrow-band-gap materials, due to the significant decrease in excited state energy (or red-shifted emission) of the CT state from donor to acceptor, or more delocalized π–π* state between weak donor and weak acceptor.[7e,10,11] Secondly, the CT state as an emissive state always leads to broadened photoluminescence (PL) and electroluminescence (EL) spectra, which is unfavourable for high

[a]*State Key Laboratory of Supramolecular Structure and Materials, Jilin University, Changchun, 130012, P. R. China. E-mail: yangbing@jlu.edu.cn; Fax: +86-431-85168502; Tel: +86-431-85193421*

[b]*College of Chemistry, Jilin University, Changchun, 130012, P. R. China*

[c]*State Key Laboratory of Luminescent Materials and Devices, Institute of Polymer Optoelectronic Materials and Devices, South China University of Technology, Guangzhou, 510640, P. R. China*

† Electronic supplementary information (ESI) available: The details of the synthesis; the ground state and excited state geometries in PPI, TPA–PPI and mTPA–PPI; absorption and emission properties of PPI, TPA–PPI and mTPA–PPI in the gas phase; detailed absorption peak positions, emission peak positions and η_{PL} values of PPI and mTPA–PPI in different solvents; HOMO and LUMO of mTPA–PPI at ground state; NTO for the $S_0 \rightarrow S_1$ absorption transition in PPI, TPA–PPI and mTPA–PPI; NTO for $S_0 \rightarrow S_n$ electronic transition character in mTPA–PPI; lifetime measurement, radiative transition rates and non-radiative transition rates of PPI and mTPA–PPI in hexane and THF solutions; low-temperature fluorescence and phosphorescence spectra of PPI and mTPA–PPI; CV curves of PPI and mTPA–PPI, and schematic diagram of design principle of mTPA–PPI; TGA and DSC graphs of PPI and mTPA–PPI; current efficiency–current density–power efficiency curves and EL spectra at different driving voltages of PPI and mTPA–PPI devices. See DOI: 10.1039/c5sc01131k

colour-purity of emission.[9g] Thirdly, the CT state usually exhibits a low efficiency fluorescence, which is attributed to the nature of the forbidden transition induced by the spatial separation between the hole and electron wavefunctions. On the contrary, the locally excited (LE) state is suited to producing high-efficiency fluorescence radiation due to the large orbital overlap.[9f,12] However, the CT state can provide a RISC channel that improves exciton-utilizing efficiency (η_s) in fluorescent OLEDs through a very small energy splitting between singlet and triplet states, which has been proven to be an effective way to utilize triplet exciton energy in fluorescent OLEDs.[8,9] Considering the above issues, if CT and LE states could be reasonably combined into one D–A molecule, it would be possible to further greatly improve the efficiency of fluorescent OLEDs. That is to say, the low-lying LE state determines the efficient fluorescence radiation, wide band-gap and colour-purity, while the high-lying CT state is responsible for the triplet exciton utilization through the RISC process. Thus, this golden combination is surely beneficial to maximize the EL efficiency of NUV OLEDs, and it can be a novel strategy to design NUV emitters with high efficiency (including high PL efficiency (η_{PL}) and high η_s) and good colour-purity by taking advantage of the D–A structure.

The *meta*-linked strategy has been adopted to construct wide-band-gap materials in prior reports, *e.g.*, *meta*-linked 3,5-bis(*N*-carbazolyl)benzene (mCP) was shown to have a short emission wavelength with high triplet energy and was used as host matrix.[13] Yang *et al.* also designed a series of *meta*-linked molecules which possessed wider optical and electrical band-gaps than their *para*-linked counterparts.[14] In this work, we designed a new NUV molecule, diphenyl-[3′-(1-phenyl-1*H*-phenanthro[9,10-*d*]imidazol-2-yl)-biphenyl-4-yl]-amine (mTPA–PPI) with a special *meta*-linked D–A structure, and it was synthesized by a one-pot cyclizing reaction followed by a Suzuki coupling reaction (Scheme 1). Compared to the *para*-linked TPA–PPI that we have already reported,[9a] not only does mTPA–PPI show shorter emission wavelength and wider band-gap, but also it possesses unique excited state properties. To rationalize our molecular design, the relationship between the molecular structures, excited state properties and EL performances are further discussed and understood by a systematic comparison among the isolated PPI, *para*-linked TPA–PPI and *meta*-linked mTPA–PPI.

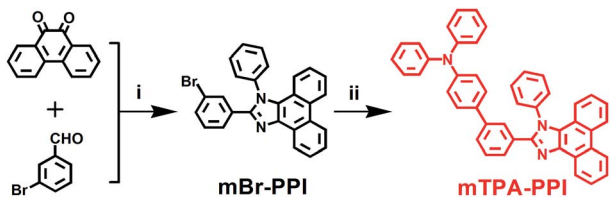

Scheme 1 Synthesis of mTPA–PPI ((i) aniline, CH_3COONH_4, CH_3-COOH, reflux under N_2 at 120 °C oil bath for 2 h; (ii) *N*,*N*-diphenyl-4-(4,4,5,5-tetramethyl-1,3,2-dioxaborolan-2-yl)aniline, Na_2CO_3, $Pd(PPh_3)_4$, toluene, C_2H_5OH, H_2O, reflux under N_2 at 90 °C oil bath for 48 h).

Results and discussion

Molecular design

Ground state and excited state geometries. As shown in Scheme 1, mTPA–PPI is composed of two moieties: triphenylamine (TPA) acts as the electron donor and 1,2-diphenyl-1*H*-phenanthro[9,10-*d*]imidazole (PPI) acts as the electron acceptor.[7c,9a] TPA is a good hole-transporting group due to its low ionization potential (IP), while PPI is a highly efficient NUV fluorophore with a very narrow full width at half maximum (FWHM).[7c,9a,15,16] We have already reported a high-efficiency blue fluorescent material TPA–PPI with the *para*-linkage between TPA and PPI, but a large red-shift was observed in emission relative to the isolated PPI as a result of the greatly extended D–A conjugation.[9a] Here, a *meta*-linked D–A architecture is adopted to break the conjugation between D and A for obtaining NUV emission from the PPI moiety, corresponding to the realization of a non-red-shifted emission upon the introduction of the CT state in the D–A system. The ground state geometries of mTPA–PPI were optimized using the density function theory (DFT-B3LYP) method at the basis set level of 6-31g(d,p). PPI is substituted with TPA at the *meta*-position of the bridging benzene ring to construct a non-collinear and twisted D–A molecule. It is noteworthy that the geometry of the PPI moiety in mTPA–PPI remains highly consistent with the isolated PPI upon the incorporation of the TPA group (Table S1†). The highest occupied molecular orbital (HOMO) and the lowest unoccupied molecular orbital (LUMO) are localized on the TPA and PPI moieties, respectively (Fig. S1†). This confirms that the *meta*-linked mode is effective in interrupting the π-conjugation between the D and A units. Thus, mTPA–PPI may be a bipolar molecule in favor of the balanced carrier transport in the light-emitting layer, in which TPA acts as a hole-transporting group and PPI as an electron-transporting group, respectively.

The excited state geometries of mTPA–PPI were also optimized using a time-dependent DFT method (TDDFT-B3LYP) at the same basis set level. From the ground state to excited state, large geometrical changes occur in the PPI moiety of mTPA–PPI, which indicates that the PPI moiety may be an active chromophore in mTPA–PPI regardless of the introduction of the TPA group. Furthermore, a very similar variation trend was observed between the PPI moiety of mTPA–PPI and the isolated PPI from the ground state to excited state. For instance, the twist angle, θ_1, between the bridging benzene and the imidazol ring is greatly decreased from 32° to 13°, which induces the more coplanar PPI moiety to be in an excited state, and the bond R_1 that connects bridging benzene with the imidazol ring is significantly shortened by about 0.04 Å. As a further comparison, from ground state to excited state, the twist angles between TPA and the bridging benzene show a more significant decrease in TPA–PPI than in mTPA–PPI, leading to a more coplanar and more rigid TPA–PPI molecular backbone than in mTPA–PPI (Table S1†).

Excited state properties. To describe the excited state properties of PPI, mTPA–PPI and TPA–PPI, the natural transition orbital (NTO) was adopted to analyze electron transition

characters for both absorption and emission, respectively (Fig. 1, Table S2 and Fig. S2†).[17] As shown in Fig. 1, both hole and particle are localized on the PPI moiety for the $S_1 \rightarrow S_0$ transition in mTPA–PPI, which are almost the same as those in isolated PPI. This indicates that the emission of the lowest singlet state (S_1) of mTPA–PPI corresponds to the pure LE state of isolated PPI *in vacuo* in the gas phase, which is also confirmed by their nearly equal emission wavelength. This just meets the requirement of our molecular design; that is, the non-red-shifted and narrow FWHM fluorescence will be maintained in mTPA–PPI upon TPA incorporation into PPI. In addition, the CT state is found to remain at a high-lying excited state, *e.g.* the S_4 state, which may contribute to a RISC channel in favor of high triplet exciton conversion (Fig. S3†). Confidently, a golden combination can be reached to maximize the EL efficiency in OLEDs: the low-lying LE state is responsible for efficient fluorescence radiation with good colour-purity, while the high-lying CT state determines the triplet exciton utilization through the RISC process. In order to elucidate the benefit of the *meta*-linkage, the NTO calculation on a *para*-linked D–A molecule (TPA–PPI) was also performed for the purpose of comparison. Both NTO hole and particle are delocalized throughout the whole TPA–PPI backbone for both the $S_0 \rightarrow S_1$ and $S_1 \rightarrow S_0$ transitions, indicating an enhanced electron delocalization for the *para*-linkage along the extended π–π^* excited state. In essence, this kind of delocalized excited state can surely result in a significant red-shift of absorption and emission relative to the LE state of PPI. As a whole, compared with PPI and TPA–PPI, mTPA–PPI may be a very suitable candidate for high-efficiency NUV materials from DFT calculations, which is expected to be validated in the following experiments.

Photophysical properties

Initially, the ultraviolet-visible (UV-vis) and PL spectra of PPI, TPA–PPI and mTPA–PPI in diluted tetrahydrofuran (THF) solutions and vacuum-evaporated films were recorded to understand their basic photophysical properties (see Fig. 2a–d). For the UV-vis spectra in Fig. 2a, obviously different from TPA–PPI, mTPA–PPI shows an absorption band around 360 nm which is not significantly strengthened relative to PPI, arising from the main LE state absorption of PPI from NTO analysis (Fig. S2†). However, upon the incorporation of TPA, mTPA–PPI shows an absorption band around 329 nm which is different from that of PPI, and some distinct characters exist at the high-lying excited states of mTPA–PPI compared to that of PPI. As a comparison, the *para*-linked TPA–PPI exhibits a significantly enhanced and broadened absorption band around 360 nm relative to PPI and mTPA–PPI, which is induced by its extended D–A conjugation or the formation of a low-lying CT state. As a consequence, due to the different linkage between TPA and PPI, mTPA–PPI makes a great difference to the excited state properties in comparison with TPA–PPI. Additionally, the optical band-gaps of PPI, mTPA–PPI and TPA–PPI in THF solutions were estimated from the onset of absorption to be 3.35 eV, 3.33 eV and 3.08 eV, respectively. From the UV-vis spectra in films (Fig. 2c), similar absorption behaviours among three compounds were also observed. Based on the above discussion, mTPA–PPI is closer to PPI in terms of absorption properties than TPA–PPI.

In Fig. 2d, the PL spectra of mTPA–PPI and PPI were measured in vacuum-evaporated film state. Both mTPA–PPI and PPI exhibit NUV emission peaking at 408 nm and 395 nm, respectively. In contrast with a single molecule in the vacuum

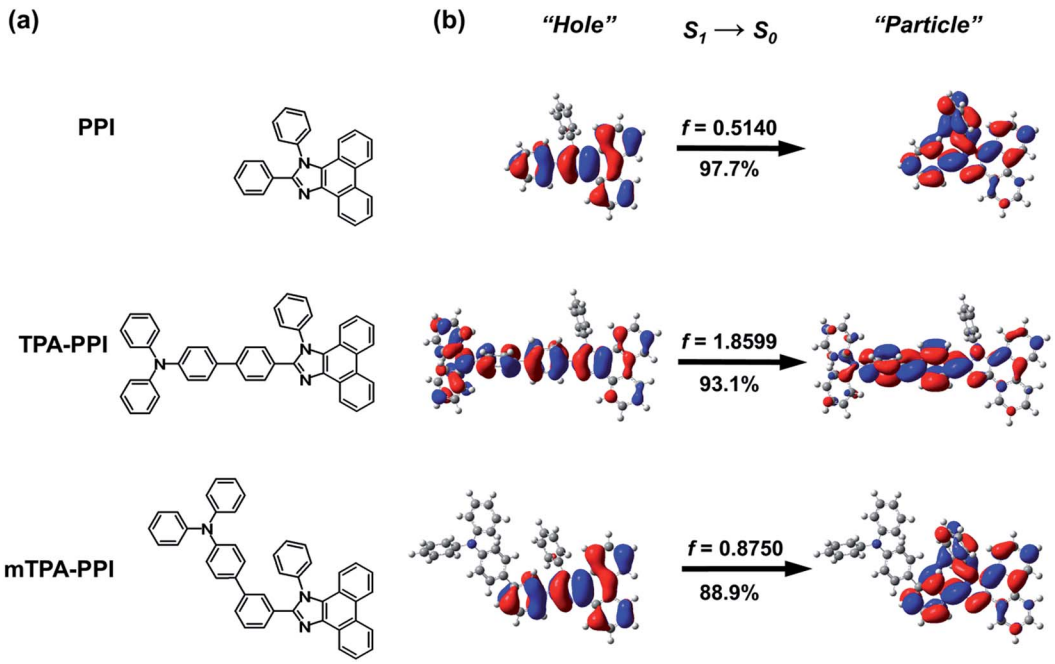

Fig. 1 (a) Molecular structures. (b) NTO for $S_1 \rightarrow S_0$ transition in PPI, TPA–PPI and mTPA–PPI. Herein, *f* represents for the oscillator strength, and the percentage weights of hole–particle are given for the $S_1 \rightarrow S_0$ emission.

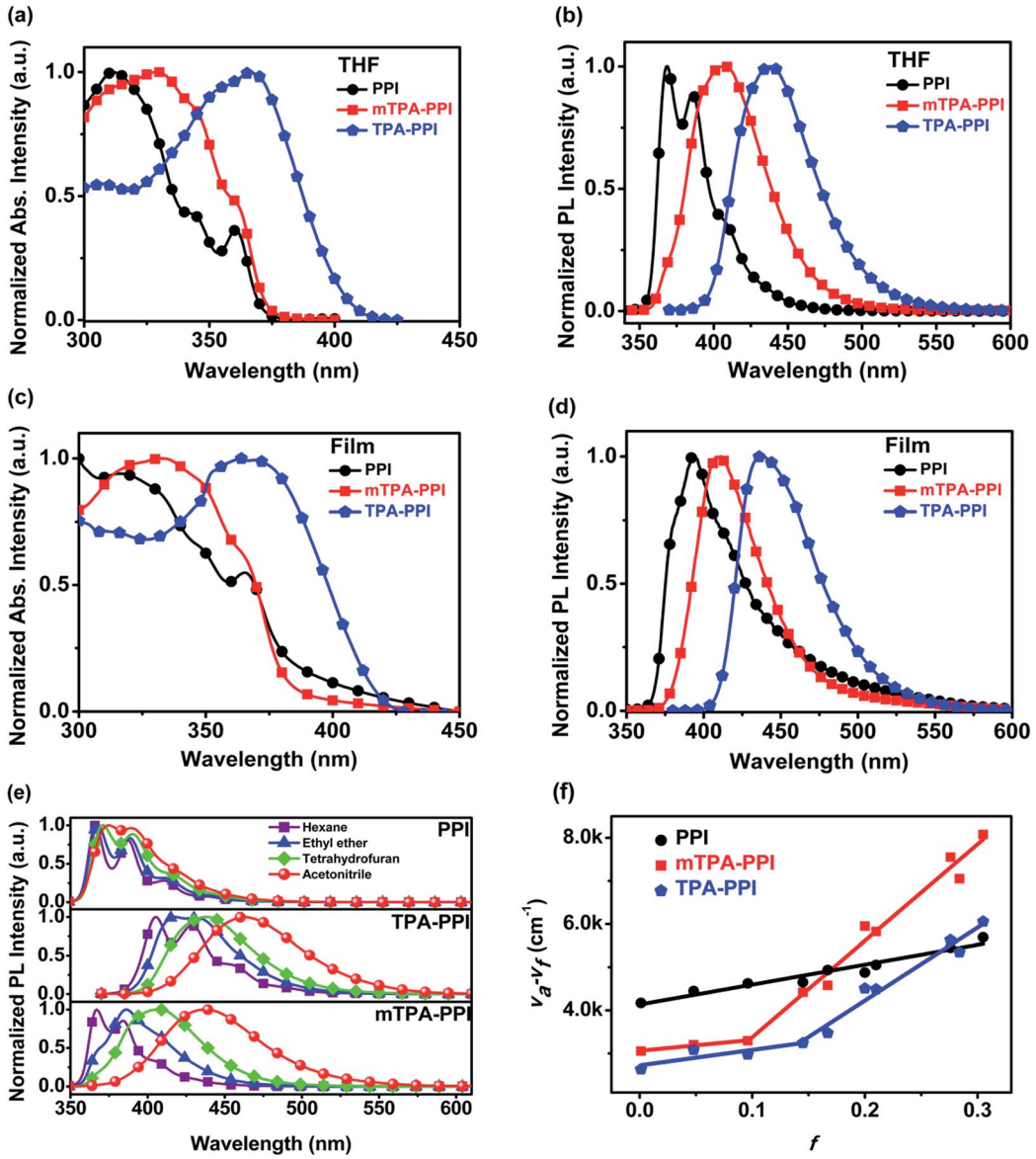

Fig. 2 (a) The UV-vis spectra of PPI, mTPA–PPI and TPA–PPI in diluted THF solutions (concentration is 1×10^{-5} mol L^{-1}). (b) The PL spectra of PPI, mTPA–PPI and TPA–PPI in diluted THF solutions (concentration is 1×10^{-5} mol L^{-1}). (c) The UV-vis spectra of PPI, mTPA–PPI and TPA–PPI in vacuum-evaporated films. (d) The PL spectra of PPI, mTPA–PPI and TPA–PPI in vacuum-evaporated films. (e) Solvatochromic PL spectra of PPI, TPA–PPI and mTPA–PPI with an increasing polarity of solvents ($f_{hexane} = 0.0012$, $f_{ethyl\ ether} = 0.167$, $f_{tetrahydrofuran} = 0.210$ and $f_{acetonitrile} = 0.305$). (f) Linear fitting of Lippert–Mataga model (the solid circles, squares and pentagons represent the Stokes shifts in different solvents, and the lines are fitted for solvatochromic models of the three compounds).

gas state, the 13 nm red-shift between mTPA–PPI and PPI can be ascribed to the solid state polarization effect.[18] In the meantime, mTPA–PPI demonstrates a narrow FWHM of 48 nm, which is very similar to 51 nm of isolated PPI. Basically, mTPA–PPI film maintains the NUV emission properties from the LE state of PPI. In fact, the η_{PL} values in evaporated films of mTPA–PPI and PPI are very close (35% and 40%, respectively). In addition, the obvious red-shift and serious trailing in the PL spectra from solvents to film suggest an occurrence of strong intermolecular aggregation in the PPI film. Nevertheless, the PL spectrum of the mTPA–PPI film is almost the same as that in THF solution, indicating that the solid state has a similar polarization effect on mTPA–PPI with that in THF (Fig. 2b). As a comparison, the TPA–PPI film shows a largely red-shifted emission at 434 nm compared with mTPA–PPI and PPI films. Consequently, the *meta*-linkage of mTPA–PPI is obviously superior to the *para*-linkage of TPA–PPI in terms of designing NUV D–A materials.

Secondly, in order to examine the excited state properties, the solvatochromic PL spectra of three compounds were systematically investigated (Fig. 2e). With the increase of solvent polarity, PPI shows almost no red-shifted PL spectra with clearly distinguished vibronic structure, corresponding to a common LE state character insensitive to the changing of polar environment. Compared with PPI, the PL spectra of *para*-

linked TPA–PPI exhibit a significant red-shift, a gradually broadened and gradually vanished vibronic resolution in PL spectra as the solvent polarity increases, indicating a typical characteristic of CT state, which is sensitive to the surroundings. Obviously, the PL peaks of TPA–PPI (405, 438, 462 nm) are greatly red-shifted relative to those of PPI (364, 369, 372 nm) from hexane, THF to acetonitrile, due to the extended D–A conjugation or the essence of low-lying CT state. Likewise, *meta*-linked mTPA–PPI also exhibits a considerable solvatochromic effect, as shown in Fig. 2e. With an increasing polarity of solvents, the PL spectra of mTPA–PPI are red-shifted and broadened, accompanied by the gradual disappearance of vibronic structure, revealing a substantial excited state transformation. Different from TPA–PPI, mTPA–PPI demonstrates nearly the same spectral shape and emission wavelengths as those of PPI in hexane, implying a highly consistent character (LE of PPI) of S_1 state. Simultaneously, η_{PL} values of PPI and mTPA–PPI are very similar in different solvents (Tables S3 and S4†).

Moreover, in order to estimate the dipole moments of the excited state (μ_e), the linear relation of the Stokes shift (ν_a–ν_f) against the orientation polarizability $f(\varepsilon,n)$ was fitted for PPI, TPA–PPI and mTPA–PPI, according to the Lippert–Mataga equation (Tables S3 and S4†).[19] From Fig. 2f, a good linear relation was obtained for PPI and μ_e was calculated to be 8.22 D through the linear slope, which indicates one single changeless emissive state as the solvent polarity increases, *i.e.*, the usual pure LE state. However, TPA–PPI displays two-section linear relations with μ_e of 9.31 D and 20.21 D, corresponding to the LE state and CT state, respectively. In the same way, mTPA–PPI also possesses a μ_e of 7.78 D for the LE state and 23.28 D for the CT state. Differently, mTPA–PPI has a smaller μ_e of the LE state and a bigger μ_e of the CT state than those of TPA–PPI, corresponding to the pure LE state character in low-polarity environments and strong CT character in high-polarity environments, respectively. Based on the facts of the same vibronic structure feature in hexane and the very close μ_e of LE state in low-polarity solvents between mTPA–PPI and PPI, it is demonstrated that the S_1 state of mTPA–PPI is in good accordance with that of PPI in low-polarity solvents. Besides, the phosphorescence spectra of PPI and mTPA–PPI were measured at 77 K, which indicated the same LE character in the lowest triplet state T_1 (Fig. S5†). In a word, the *meta*-linked mode is feasible for realization of a non-red-shifted LE emission under the precondition of the introduction of a CT state through D–A architecture.

Electrochemical and thermal properties

As a candidate for a NUV emitter, the electrochemical properties of mTPA–PPI were measured by cyclic voltammetry (CV) together with PPI for the purpose of comparison. Basically, the two compounds display almost the same LUMO levels (−2.02 eV for PPI and −2.09 eV for mTPA–PPI) resulting from their identical PPI group (Table 1 and Fig. S6a†). Nevertheless, the HOMO level of mTPA–PPI is greatly raised up to −5.23 eV relative to −5.58 eV in PPI, as a result of TPA acting as an electron donor to dominate electrochemical oxidation of mTPA–PPI. Although mTPA–PPI and PPI possess almost the same optical band-gaps, the electrochemical measurements present quite different electrical band-gaps, 3.56 eV for PPI and 3.14 eV for mTPA–PPI, respectively. For the reason of separation of optical and electrical band-gaps, the HOMO and LUMO of mTPA–PPI are separated and distributed over donor (TPA moiety) and acceptor (PPI moiety), respectively, which leads to forbidden electronic transitions, while both the HOMO−1 and LUMO of mTPA–PPI share large orbital overlap almost distributed over the PPI moiety of mTPA–PPI, which results in allowed electronic transitions (Fig. S6b†).[20] Thus, the optical band-gap of mTPA–PPI is consistent with that of PPI.

Additionally, the thermal properties of light-emitting materials are also a key factor affecting device stability. For mTPA–PPI, the glass transition temperature (T_g) and thermal decomposition temperature (T_d) were measured as 120 °C and 467 °C, which were much higher than 64 °C and 348 °C of PPI, respectively (Table 1 and Fig. S7†). As we expected, mTPA–PPI exhibits much better thermal stability than its parent molecule PPI on the premise of unchanged emission colour, which will be in favour of NUV OLED stability.

Electroluminescence performances

To evaluate the EL performance of NUV material mTPA–PPI as an emitter, non-doped OLEDs were fabricated with a multilayer device structure (Fig. 3a): ITO/MoO_3 (7 nm)/*N*,*N*′-di-1-naphthyl-*N*,*N*′-diphenylbenzidine (NPB) (80 nm)/4,4′,4″-tri(*N*-carbazolyl)-triphenylamine (TCTA) (5 nm)/mTPA–PPI or PPI (20 nm)/1,3,5-tri(phenyl-2-benzimidazolyl)-benzene (TPBi) (40 nm)/LiF (1 nm)/Al (100 nm). The PPI OLED performance was also estimated with the same device structure for the purpose of comparison, and these two EL device performances are summarized in Table 2. Firstly, the mTPA–PPI device has a lower turn-on voltage of 3.2 V (recorded at the luminance of 1 cd m^{-2}) than the 3.8 V of PPI device, which can be ascribed to the easier hole injection in mTPA–PPI due to the incorporation of the TPA group. Secondly, the PPI device demonstrates a maximum luminous efficiency of 0.71 cd A^{-1} and a maximum luminance of 3307 cd m^{-2} (Fig. S8a† and 3b).

Compared with PPI, the mTPA–PPI device shows a higher maximum luminous efficiency of 0.84 cd A^{-1} and a larger maximum luminance of 4065 cd m^{-2} (Fig. S8c† and 3b). Based on the EQE-luminance characteristics of the two devices (Fig. 3c), the mTPA–PPI device harvests a maximum EQE of 3.33%, which is significantly higher than that of the PPI device

Table 1 The electrochemical and thermal properties of PPI and mTPA–PPI

Materials	T_g[a] (°C)	T_d[b] (°C)	HOMO[c] (eV)	LUMO[c] (eV)	E_g[d] (eV)
PPI	64	348	−5.58	−2.02	3.56
mTPA–PPI	120	467	−5.23	−2.09	3.14

[a] T_g is glass-transition temperature. [b] T_d is thermal-decomposition temperature at a weight percentage of 95%. [c] HOMO and LUMO levels were measured based on ferrocene as reference (Fc) (4.8 eV). [d] E_g (eV) = LUMO (eV) − HOMO (eV).

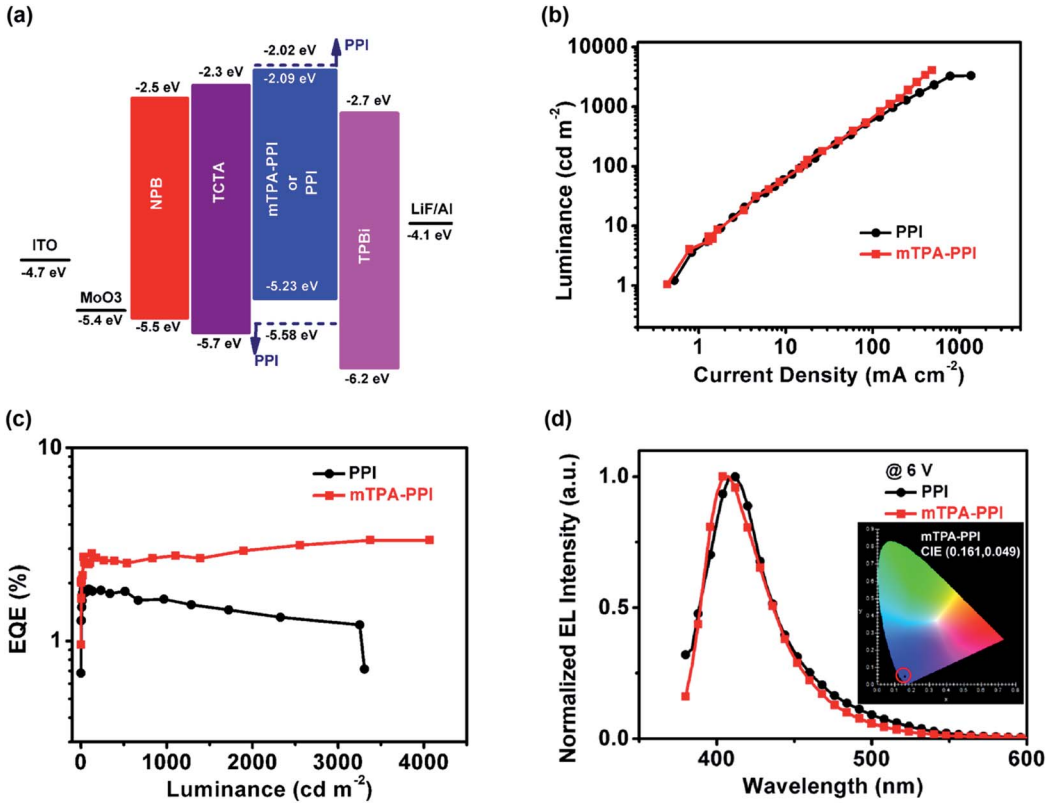

Fig. 3 (a) Schematic energy level diagram of PPI and mTPA–PPI devices (dashed lines represent the HOMO and LUMO levels of PPI). (b) Luminance *versus* current density curves of PPI and mTPA–PPI devices. (c) External quantum efficiency *versus* luminance curves of PPI and mTPA–PPI devices. (d) EL spectra of a multilayered OLED based on PPI and mTPA–PPI as the emitters (the inset graph shows CIE coordinate of mTPA–PPI at 6 V).

(1.86%). In the meantime, the mTPA–PPI device exhibits the more excellent operational stability without roll-off but gradual ascent on EQE with increasing luminance. Furthermore, the η_s can be estimated for both mTPA–PPI and PPI devices on the basis of the known η_{PL} values, maximum EQEs and the two assumed parameters of the light out-coupling efficiency of 20% and the 100% hole–electron recombination in the OLEDs. Thus, the $\eta_s = 48\%$ in the mTPA–PPI device is obtained, which breaks through the limit of $\eta_s = 25\%$ for conventional fluorescent OLEDs and is a two-fold increase relative to 23% in the PPI device. For the high η_s of mTPA–PPI device, the possibilities of triplet–triplet annihilation (TTA) and thermally activated delayed fluorescence (TADF) seem to be excluded, in view of the linear growth of the luminance–current density curve and the large energy distance ($\Delta E_{ST} \approx 0.76$ eV) between S_1 and T_1 (ΔE_{ST} was estimated from the maximum peak of the low-temperature fluorescence spectrum and the first vibronic peak of the low-temperature phosphorescence spectrum).[8,21] Considering the nano-second timescale mono-exponential lifetime (Fig. S4†) and the high-lying CT state RISC channel in mTPA–PPI, we suppose the high η_s of mTPA–PPI could be attributed to the triplet exciton contribution from the RISC process along the possible "hot exciton" channel.[9]

What is more, the mTPA–PPI device exhibits very excellent NUV EL with a Commission Internationale de L'Eclairage (CIE) coordinate of (0.161, 0.049), and its EL peak value is at 404 nm with a narrow FWHM of only 47 nm, which is of very good colour-purity, as shown in Fig. 3d (our instrument, a PR-650 Spectroscan spectrometer, cannot detect the EL luminance signal below 380 nm). Interestingly, the EL spectrum of mTPA–PPI has almost the same maximum wavelength as PL in an evaporated film and no obvious trailing at long wavelengths, indicating that the formation of an excimer or exciplex can be effectively suppressed in the EL process, other than some wide-

Table 2 The comparison of device performances between PPI and mTPA–PPI

Emitters	$\lambda_{EL,max}$[a] (nm)	CIE[b] (x, y)	$V_{turn\text{-}on}$[c] (V)	LE_{max}[d] (cd A^{-1})	PE_{max}[e] (lm W^{-1})	EQE_{max}[f] (%)	L_{max}[g] (cd m^{-2})
PPI	412	(0.161, 0.065)	3.8	0.71	0.40	1.86	3307
mTPA–PPI	404	(0.161, 0.049)	3.2	0.84	0.48	3.33	4065

[a] Maximum peak of EL spectra. [b] Measured at 6 V. [c] Turn-on voltage recorded at the luminance of 1 cd m^{-2}. [d] Maximum luminous efficiency. [e] Maximum power efficiency. [f] Maximum external quantum efficiency. [g] Maximum luminance.

band-gap light-emitting materials based devices.[7e,22] It can be attributed to the branched *meta*-linkage that prevents it from having strong intermolecular interactions in the light-emitting layer and its interfaces due to the twisted molecular backbone in mTPA–PPI. Also, the EL spectra of the mTPA–PPI device are surely independent of driving voltages from 4 V to 9 V, revealing that the recombination of electrons and holes is well confined within the emitter layer during the EL process (Fig. S8d†). As a contrast, the PPI device also shows a NUV emission at 412 nm with a FWHM of 48 nm and a CIE coordinate of (0.161, 0.065), but it is really inferior to that of mTPA–PPI (the EL spectra under driving voltages from 4 V to 8 V are shown in Fig. S8b†). The inferior performance of the PPI device probably derives from the close packing of the PPI molecules in the light-emitting layer and the strong intermolecular interactions at the interfaces, as a result of the small volume and planar structure of PPI.

Above all, to the best of our knowledge, mTPA–PPI is among the best NUV materials that have ever been reported, and exhibits a combination of a high-efficiency NUV EL, a narrow FWHM and a small *y*-value of CIE coordinate.[3d,6] Key data of the mTPA–PPI-based device and other high-performance violet/NUV light-emitting devices with EL wavelengths below 410 nm are listed together in Table S5† for the purpose of comparison. The superior device performances of mTPA–PPI could be ascribed to the following facts: (i) the *meta*-linkage of mTPA–PPI gives rise to a LE emission like PPI, which inherits high η_{PL} and good colour-purity of the parent PPI; (ii) the introduction of a high-lying CT state promotes a RISC process to enhance η_s in the mTPA–PPI device; (iii) the rising HOMO level facilitates easier hole injection in the mTPA–PPI layer due to the incorporation of TPA. Therefore, this *meta*-linkage between D and A is an ideal strategy to design next generation NUV materials for high-efficiency PL, high-efficiency exciton utilization and colour-purity OLEDs.

Conclusions

In summary, a special *meta*-linkage was adopted to construct a NUV D–A molecule, mTPA–PPI, in an attempt to harmonize a common conflict between the non-red-shifted emission and the introduction of the CT state in the D–A system. Quantum chemical calculations revealed that mTPA–PPI could be a very suitable candidate for a high-efficiency NUV material, which possessed nearly the same LE state character and non-red-shifted emission relative to that of the isolated PPI. Furthermore, the following photophysical experiments confirmed the molecular design concept as mentioned above. The mTPA–PPI exhibited consistent PL spectra with those of isolated PPI in low-polarity solvents, and the solvatochromic effect demonstrated the coexistence of a low-lying LE state and high-lying CT state as we expected. Finally, the mTPA–PPI device exhibited high-efficiency and colour-purity NUV OLED performance: a very high maximum EQE of 3.33% corresponding to a η_s of 48%, and a CIE coordinate of (0.161, 0.049) originating from an EL spectrum peaking at 404 nm with a narrow FWHM of 47 nm. This result is among the best for NUV OLEDs, with the top efficiency of all current records. In nature, a golden combination of excited states is responsible for the high-performance EL: the low-lying LE state contributes to high-efficiency, non-red-shifted and good colour-purity PL, while the high-lying CT state enables high exciton utilization. Our results demonstrate the *meta*-linked D–A systems may be an excellent type of EL material to achieve NUV OLEDs with high efficiency and favourable colour-purity.

Acknowledgements

This work is supported by the National Natural Science Foundation of China (51273078, 51473063 and 91233113), the Ministry of Science and Technology of China (2013CB834801 and 2015CB655003) and the Graduate Innovation Fund of Jilin University (Project 2014011).

Notes and references

1 J. Shinar and R. J. Shinar, *J. Phys. D: Appl. Phys.*, 2008, **41**, 133001.
2 H. V. Santen and J. H. M. Neijzen, *Jpn. J. Appl. Phys.*, 2003, **42**(1), 1110.
3 (*a*) A. Kraft, A. C. Grimsdale and A. B. Holmes, *Angew. Chem., Int. Ed.*, 1998, **37**, 402; (*b*) D. F. O'Brien, M. A. Baldo, M. E. Thompson and S. R. Forrest, *Appl. Phys. Lett.*, 1999, **74**, 442; (*c*) S. J. Yeh, M. F. Wu, C. T. Chen, Y. H. Song, Y. Chi, M. H. Ho, S. F. Hsu and C. H. Chen, *Adv. Mater.*, 2005, **17**, 285; (*d*) T.-C. Chao, Y.-T. Lin, C.-Y. Yang, T. S. Hung, H.-C. Chou, C.-C. Wu and K.-T. Wong, *Adv. Mater.*, 2005, **17**, 992.
4 (*a*) C. W. Tang and S. A. VanSlyke, *Appl. Phys. Lett.*, 1987, **51**, 913; (*b*) M. A. Baldo, D. F. O'Brien, Y. You, A. Shoustikov, S. Sibley, M. E. Thompson and S. R. Forrest, *Nature*, 1998, **395**, 151; (*c*) M. T. Lee, C. H. Liao, C. H. Tsai and C. H. Chen, *Adv. Mater.*, 2005, **17**, 2493; (*d*) Y. Sun, N. C. Giebink, H. Kanno, B. Ma, M. E. Thompson and S. R. Forrest, *Nature*, 2006, **440**, 908; (*e*) S. J. Lee, J. S. Park, K. J. Yoon, Y. I. Kim, S. H. Jin, S. K. Kang, Y. S. Gal, S. Kang, J. Y. Lee, J. W. Kang, S. H. Lee, H. D. Park and J. J. Kim, *Adv. Funct. Mater.*, 2008, **18**, 3922.
5 (*a*) Y. Y. Lyu, J. H. Kwak, O. Kwon, S. H. Lee, D. Kim, C. H. Lee and K. Char, *Adv. Mater.*, 2008, **20**, 2720; (*b*) Y. Park, J. H. Lee, D. H. Jung, S. H. Liu, Y. H. Lin, L. Y. Chen, C. C. Wud and J. Park, *J. Mater. Chem.*, 2010, **20**, 5930; (*c*) S. W. Culligan, A. C. A. Chen, J. U. Wallace, K. P. Klubek, C. W. Tang and S. H. Chen, *Adv. Funct. Mater.*, 2006, **16**, 1481; (*d*) M. H. Ho, Y. S. Wu, S. W. Wen, M. T. Lee, T. M. Chen, C. H. Chen, K. C. Kwok, S. K. So, K. T. Yeung, Y. K. Cheng and Z. Q. Gao, *Appl. Phys. Lett.*, 2006, **89**, 252903; (*e*) A. L. Fisher, K. E. Linton, K. T. Kamtekar, C. Pearson, M. R. Bryce and M. C. Petty, *Chem. Mater.*, 2011, **23**, 1640.
6 (*a*) K. Okumoto and Y. Shirota, *Appl. Phys. Lett.*, 2001, **79**, 1231; (*b*) S. Tang, M. Liu, P. Lu, H. Xia, M. Li, Z. Q. Xie, T. Z. Shen, C. Gu, H. P. Wang, B. Yang and Y. G. Ma, *Adv. Funct. Mater.*, 2007, **17**, 2869; (*c*) Y. Yang, P. Cohn, S. H. Eom, K. A. Abboud, R. K. Castellano and J. Xue, *J.*

Mater. Chem. C, 2013, **1**, 2867; (*d*) K. Guo, J. Zhang, T. Xu, X. Gao and B. Wei, *J. Disp. Technol.*, 2014, **10**, 642; (*e*) X. Tang, L. Yao, H. Liu, F. Shen, S. Zhang, Y. Zhang, H. Zhang, P. Lu and Y. Ma, *J. Mater. Chem. C*, 2014, **2**, 5019.

7 (*a*) T. H. Huang, J. T. Lin, L. Y. Chen, Y. T. Lin and C. C. Wu, *Adv. Mater.*, 2006, **18**, 602; (*b*) M. Y. Lai, C. H. Chen, W. S. Huang, J. T. Lin, T. H. Ke, L. Y. Chen, M. H. Tsai and C. C. Wu, *Angew. Chem., Int. Ed.*, 2008, **47**, 581; (*c*) Y. Zhang, S.-L. Lai, Q.-X. Tong, M.-F. Lo, T.-W. Ng, M.-Y. Chan, Z.-C. Wen, J. He, K.-S. Jeff, X.-L. Tang, W.-M. Liu, C.-C. Ko, P.-F. Wang and C.-S. Lee, *Chem. Mater.*, 2012, **24**, 61; (*d*) J. Ye, Z. Chen, M.-K. Fung, C. Zheng, X. Ou, X. Zhang, Y. Yuan and C.-S. Lee, *Chem. Mater.*, 2013, **25**, 2630; (*e*) Y. Yuan, J.-X. Chen, F. Lu, Q.-X. Tong, Q.-D. Yang, H.-W. Mo, T.-W. Ng, F.-L. Wong, Z.-Q. Guo, J. Ye, Z. Chen, X.-H. Zhang and C.-S. Lee, *Chem. Mater.*, 2013, **25**, 4957.

8 (*a*) T. Nakagawa, S. Y. Ku, K. T. Wong and C. Adachi, *Chem. Commun.*, 2012, **48**, 9580; (*b*) H. Uoyama, K. Goushi, K. Shizu, H. Nomura and C. Adachi, *Nature*, 2012, **492**, 234; (*c*) S. Y. Lee, T. Yasuda, H. Nomura and C. Adachi, *Appl. Phys. Lett.*, 2012, **101**, 093306; (*d*) G. Mehes, H. Nomura, Q. Zhang, T. Nakagawa and C. Adachi, *Angew. Chem., Int. Ed.*, 2012, **51**, 11311; (*e*) H. Tanaka, K. Shizu, H. Miyazaki and C. Adachi, *Chem. Commun.*, 2012, **48**, 11392; (*f*) Q. Zhang, J. Li, K. Shizu, S. Huang, S. Hirata, H. Miyazaki and C. Adachi, *J. Am. Chem. Soc.*, 2012, **134**, 14706; (*g*) H. Nakanotani, K. Masui, J. Nishide, T. Shibata and C. Adachi, *Sci. Rep.*, 2013, **3**, 2127; (*h*) Q. Zhang, B. Li, S. Huang, H. Nomura, H. Tanaka and C. Adachi, *Nat. Photonics*, 2014, **8**, 326.

9 (*a*) W. Li, D. Liu, F. Shen, D. Ma, Z. Wang, T. Feng, Y. Xu, B. Yang and Y. Ma, *Adv. Funct. Mater.*, 2012, **22**, 2797; (*b*) S. Zhang, W. Li, L. Yao, Y. Pan, F. Shen, R. Xiao, B. Yang and Y. Ma, *Chem. Commun.*, 2013, **49**, 11302; (*c*) Y. Pan, W. Li, S. Zhang, L. Yao, C. Gu, H. Xu, B. Yang and Y. Ma, *Adv. Opt. Mater.*, 2014, **2**, 510; (*d*) W. Li, Y. Pan, L. Yao, H. Liu, S. Zhang, C. Wang, F. Shen, P. Lu, B. Yang and Y. Ma, *Adv. Opt. Mater.*, 2014, **2**, 892; (*e*) L. Yao, S. Zhang, R. Wang, W. Li, F. Shen, B. Yang and Y. Ma, *Angew. Chem., Int. Ed.*, 2014, **53**, 2119; (*f*) W. Li, Y. Pan, R. Xiao, Q. Peng, S. Zhang, D. Ma, F. Li, F. Shen, Y. Wang, B. Yang and Y. Ma, *Adv. Funct. Mater.*, 2014, **24**, 1609; (*g*) W. Li, L. Yao, H. Liu, Z. Wang, S. Zhang, R. Xiao, H. Zhang, P. Lu, B. Yang and Y. Ma, *J. Mater. Chem. C*, 2014, **2**, 4733; (*h*) S. Zhang, L. Yao, Q. Peng, W. Li, Y. Pan, R. Xiao, Y. Gao, C. Gu, Z. Wang, P. Lu, F. Li, S. Su, B. Yang and Y. Ma, *Adv. Funct. Mater.*, 2015, **25**, 1755.

10 H. H. Chou and C. H. Cheng, *Adv. Mater.*, 2010, **22**, 2468.

11 (*a*) G. Qian and Z. Y. Wang, *Can. J. Chem.*, 2010, **88**, 192; (*b*) M. T. Sharbati, F. Panahi and A. Gharavi, *IEEE Photonics Technol. Lett.*, 2010, **22**, 1695; (*c*) A. Thomas, K. Bhanuprakash and K. M. M. K. Prasad, *J. Phys. Org. Chem.*, 2011, **24**, 821; (*d*) Y. L. Liao, C. Y. Lin, K. T. Wong, T. H. Hou and W. Y. Hung, *Org. Lett.*, 2007, **9**, 4511; (*e*) W. Z. Yuan, Y. Gong, S. Chen, X. Y. Shen, J. W. Y. Lam, P. Lu, Y. Lu, Z. Wang, R. Hu, N. Xie, H. S. Kwok, Y. Zhang, J. Z. Sun and B. Z. Tang, *Chem. Mater.*, 2012, **24**, 1518; (*f*) X. Chen, G. Zhang, H. Luo, Y. Li, Z. Liu and D. Zhang, *J. Mater. Chem. C*, 2014, **2**, 2869.

12 A. D. Gorse and M. Pesquer, *J. Phys. Chem.*, 1995, **99**, 4039.

13 V. Adamovich, J. Brooks, A. Tamayo, A. M. Alexander, P. I. Djurovich, B. W. D'Andrade, C. Adachi, S. R. Forrest and M. E. Thompson, *New J. Chem.*, 2002, **26**, 1171.

14 H. Huang, Y. Wang, S. Zhuang, X. Yang, L. Wang and C. Yang, *J. Phys. Chem. C*, 2012, **116**, 19458.

15 (*a*) B. Yang, S.-K. Kim, H. Xu, Y.-I. Park, H. Zhang, C. Gu, F. Shen, C. Wang, D. Liu, X. Liu, M. Hanif, S. Tang, W. Li, F. Li, J. Shen, J.-W. Park and Y. Ma, *ChemPhysChem*, 2008, **9**, 2601; (*b*) S.-K. Kim, B. Yang, Y. Ma, J.-H. Lee and J.-W. Park, *J. Mater. Chem.*, 2008, **18**, 3376; (*c*) S.-K. Kim, B. Yang, Y.-I. Park, Y. Ma, J.-Y. Lee, H.-J. Kim and J. Park, *Org. Electron.*, 2009, **10**, 822; (*d*) S. Tang, W. Li, F. Shen, D. Liu, B. Yang and Y. Ma, *J. Mater. Chem.*, 2012, **22**, 4401.

16 (*a*) Z. Wang, P. Lu, S. Chen, Z. Gao, F. Shen, W. Zhang, Y. Xu, H. S. Kwok and Y. Ma, *J. Mater. Chem.*, 2011, **21**, 5451; (*b*) H. Huang, Y. Wang, B. Wang, S. Zhuang, B. Pan, X. Yang, L. Wang and C. Yang, *J. Mater. Chem. C*, 2013, **1**, 5899; (*c*) M. R. Zhu and C. Yang, *Chem. Soc. Rev.*, 2013, **42**, 4963; (*d*) Z. Gao, Y. Liu, Z. Wang, F. Shen, H. Liu, G. Sun, L. Yao, Y. Lv, P. Lu and Y. Ma, *Chem.–Eur. J.*, 2013, **19**, 2602; (*e*) Z. Wang, Y. Feng, H. Li, Z. Gao, X. Zhang, P. Lu, P. Chen, Y. Ma and S. Liu, *Phys. Chem. Chem. Phys.*, 2014, **16**, 10837; (*f*) Z. Gao, Z. Wang, T. Shan, Y. Liu, F. Shen, Y. Pan, H. Zhang, X. He, P. Lu, B. Yang and Y. Ma, *Org. Electron.*, 2014, **15**, 2667; (*g*) Z. Gao, G. Cheng, F. Shen, S. Zhang, Y. Zhang, P. Lu and Y. Ma, *Laser Photonics Rev.*, 2014, **8**, L6.

17 R. L. Martin, *J. Chem. Phys.*, 2003, **118**, 4775.

18 (*a*) J. E. Norton and J.-L. Bredas, *J. Am. Chem. Soc.*, 2008, **130**, 12377; (*b*) S. M. Ryno, C. Risko and J.-L. Bredas, *J. Am. Chem. Soc.*, 2014, **136**, 6421.

19 Z. R. Grabowski, K. Rotkiewicz and W. Rettig, *Chem. Rev.*, 2003, **103**, 3899.

20 D. Hu, F. Shen, H. Liu, P. Lu, Y. Lv, D. Liu and Y. Ma, *Chem. Commun.*, 2012, **48**, 3015.

21 C.-J. Chiang, A. Kimyonok, M. K. Etherington, G. C. Griffiths, V. Jankus, F. Turksoy and A. P. Monkman, *Adv. Funct. Mater.*, 2013, **23**, 739.

22 (*a*) C. Liu, Y. Li, Y. Li, C. Yang, H. Wu, J. Qin and Y. Cao, *Chem. Mater.*, 2013, **25**, 3320; (*b*) C. Liu, Q. Fu, Y. Zou, C. Yang, D. Ma and J. Qin, *Chem. Mater.*, 2014, **26**, 3074.

